PHYSICAL REVIEW B VOLUME 27, NUMBER 12 15 JUNE 1983

Structural, elastic, and transport anomalies in molybdenum/nickel superlattices

Mahbub R. Khan, C. S. L. Chun, G. P. Felcher, M. Grimsditch, A. Kueny,*
Charles M. Falco,† and Ivan K. Schuller
Materials Science and Technology Division, Argonne National Laboratory, Argonne, Illinois 60439
(Received 10 November 1982)

Metallic superlattices of nickel and molybdenum have been synthesized for a wide range of layer thicknesses by alternate sputtering. X-ray examination shows that they are composed of layers of fcc nickel and bcc molybdenum oriented along [111] and [110] directions, respectively. Anomalies have been observed in the lattice spacings, elastic moduli, and electrical resistivity versus modulation wavelength. These anomalies occur simultaneously at the same superlattice wavelength. The anomalies have been interpreted as due to strains in the nickel lattice.

I. INTRODUCTION

The production and stabilization of new materials that do not occur naturally is a problem of much current interest. Thin-film deposition techniques (molecular beam epitaxy and sputtering) are being extensively exploited for the preparation of semiconductor[1] and metallic[2] superlattices. Most work to date has been performed on combinations of materials that form solid solutions[2,3] and that are lattice-matched. However, recent work[4,5] shows that it is also possible to stabilize superlattice structures in materials that have a eutectic binary-phase diagram and do not have matching lattice parameters. These structures are found to exhibit a variety of interesting physical phenomena.[6–17] At present, it is not clear what material and preparation parameters predetermine the growth of a superstructure in certain metals while precluding such growth in others. Consequently, it is still necessary to explore a wide range of parameters for different combinations of metals that form superlattices. In addition, it is important to know if the different physical properties are universal or structure dependent.

In the present paper we describe the structure, elastic behavior, and electrical resistivity of Mo/Ni superlattices with the goal of defining stability conditions of a superstructure made of components with significantly different atomic radii and individually crystallizing in different symmetries (bcc and fcc). We should stress that Mo and Ni have a noneutectic equilibrium binary-phase diagram in contrast to the eutectic Nb-Cu system.[18] A forthcoming paper is planned to address the magnetic properties of Mo/Ni superlattices.

II. SAMPLE PREPARATION

Mo/Ni multilayered samples were prepared by sequential sputter deposition of Mo and Ni using a technique described earlier.[4] Briefly, the material is sputtered from two high-rate Magnetron sputtering guns which are shielded from each other so that no overlap of the two particle beams occurs. The substrates used for the studies reported here [90° and 0° sapphire, MgO, NaCl, mica, glass, Ge(111), Ge(100), Si(111), Si(100), KCl, and BaF_2] were held on a temperature-controlled (±2 °C), heated (20 °C −350 °C), rotating table which could move them from one beam of particles to the other.

A systematic search was performed on the twelve different substrates as a function of sputtering rate, pressure, and substrate temperature in order to obtain a high degree of texture and possibly epitaxy. The highest degree of texture was found for substrates of mica, 90° sapphire, and Si(111) single crystals held at room temperature while sputtering in a 15-mTorr argon atmosphere at a rate of 10–30 Å/sec. Table I shows the degree of texture on these three substrates. All samples referred to in this paper were prepared under the conditions given above. After we determined the conditions for the highest degree of texture, equal layer (5–5000 Å) thickness samples were prepared at a constant 30-Å/sec sputtering rate by varying only the rotation speed of the platform while all other parameters were kept constant. The unequal layer thicknesses were prepared by fixing the relative rates of Mo and Ni at 3:1 or 1:3 and only varying the rotation speed from sample to sample.

The modulation wavelength Λ was determined by

TABLE I. Intensity ratios of x-ray peaks observed for pure Mo films or pure Ni films on substrates which produce the highest degree of texture.

Intensity ratio	Mica	90° sapphire	Si[111]
I(Mo[110])/I(Mo[211])	10	39	8.1
I(Ni[111])/I(Ni[200])	88	37	7

dividing the total thickness of the sample (~ 1 μm, measured with a calibrated Sloan Dektak surface profiler) by the total number of revolutions of the sample platform during the deposition and independently by computing the individual layer thickness from the sputtering rate (measured with a quartz-crystal oscillator), the size of the sputtering beam, and the time the substrate spent over each beam. For modulation wavelengths between 16 and 200 Å, Λ was also calculated using standard x-ray diffraction methods. In the common region the layer thickness obtained from all three measurements agreed to better than 5%.

III. CRYSTALLOGRAPHY

Standard x-ray diffraction using Cu $K\alpha$ radiation was used to determine the structure of the films. Figure 1 shows the x-ray intensities obtained for equal layer thickness samples when examined in the θ–2θ reflection geometry. For large values of the layer thickness ($\Lambda/2$) two lines appear, corresponding to the (110) crystal plane of molybdenum ($d_{\mathrm{Mo}}=2.220$ Å) and the (111) plane of nickel ($d_{\mathrm{Ni}}=2.030$ Å). For lower values of Λ the structure is composed of a central line which corresponds to an average interatomic spacing $\bar{d}$ surrounded by modulation satellites of order n at

$$2\frac{\sin\theta}{\lambda_x}=\frac{1}{\bar{d}}\pm\frac{n}{\Lambda}\ . \tag{1}$$

For $\Lambda \geq 200$ Å the x-ray peaks are relatively broad because the satellite peaks are not resolved. For 130 Å $\geq \Lambda \geq 16.6$ Å the x-ray peaks are reasonably sharp, indicating good crystallization perpendicular to the layers; below 16.6 Å only one rather broad line appears, indicating that a long-range crystalline order is no longer maintained. This could be due to agglomeration in the Ni layers, alloying, or a structural change in either of the constituents. Figure 1 shows the results obtained for samples grown on 90° sapphire substrates. In this reflection geometry, the x-ray results are practically indistinguishable from those obtained from samples grown on mica and (111) silicon wafers. Similar results are also obtained for unequal layer thicknesses of nickel and molybdenum (Fig. 2).

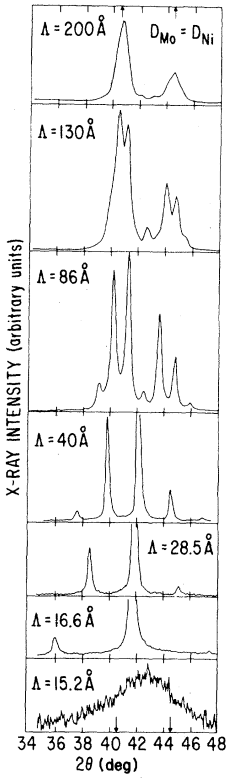

FIG. 1. θ–2θ x-ray diffraction intensity spectra for equal layer thickness Mo/Ni superlattice samples.

The x-ray results presented in Figs. 1 and 2 can be explained in terms of a structure which consists of alternating layers of (111) fcc nickel planes and (110) bcc molybdenum planes. This is the type of growth observed for a *thick* (> 2000 Å) molybdenum film on nickel and a *thick* (> 2000 Å) nickel film on molybdenum. This structure is identical to that used earlier to describe Nb(bcc)/Cu(fcc) superlattices.[5]

For a quantitative determination of the modulation shape, an analysis of the reflection manifolds in Figs. 1 and 2 was carried out. The experimental intensities were reduced[19] by the Lorentz, absorption, polarization, etc., factors to yield $c\,|F|^2$, where c is a normalization constant obtained by setting the sum of the reduced intensities of each manifold equal to one and F is the structure factor. The structure factor can be calculated from the planar scattering amplitudes of Ni and Mo, the respective number of planes, and their phases. Since in the transmission geometry x-ray spectra to be described later we found no major changes of the inplane structure, the planar scattering amplitudes were tak-

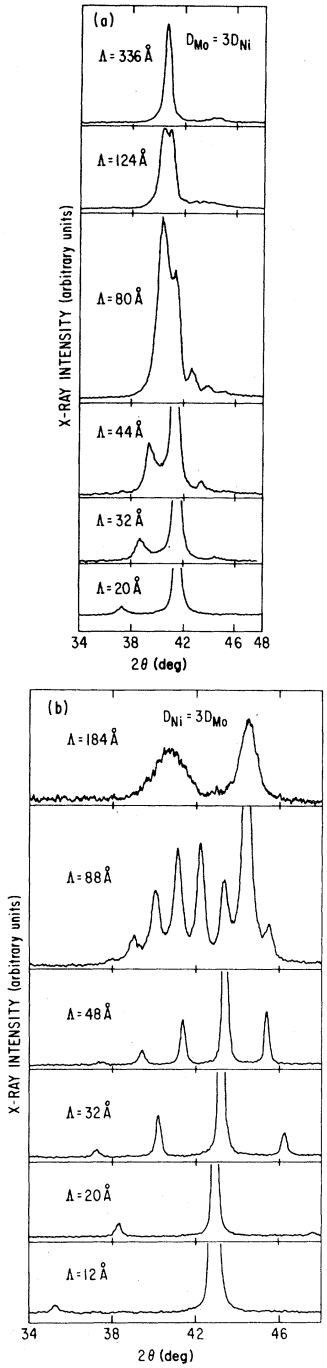

FIG. 2. θ–2θ x-ray diffraction intensity spectra for superlattices with (a) Mo layers 3 times thicker than Ni layers and (b) Ni layers 3 times thicker than Mo layers.

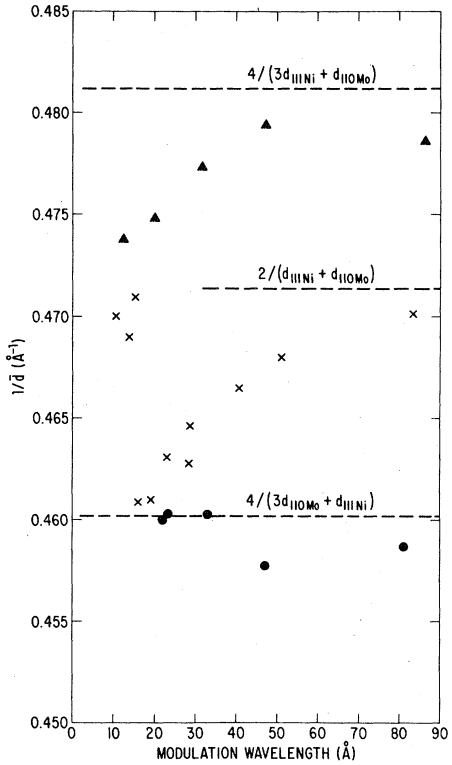

FIG. 3. Reciprocal of the average lattice spacing $\bar{d}$ vs modulation wavelength. Triangles, $D_{Ni}=3D_{Mo}$; crosses, $D_{Ni}=D_{Mo}$; dots, $3D_{Ni}=D_{Mo}$.

en to be those found in the bulk for Ni(111) and Mo(110) planes.[20]

The relative phases are not as well known since the experimental line position only determines the average spacing $\bar{d}$ which is given by

$$\bar{d}=\frac{\sum_{i=1}^{n_1} d_{1i}+\sum_{i=1}^{n_2} d_{2i}}{n_1+n_2}, \tag{2}$$

where n_1, d_{1i}, n_2, and d_{2i} are the number and spacing of Ni(111) and Mo(110) planes in each layer and the summation is carried over one superlattice period. Figure 3 shows the experimentally determined average lattice spacing $1/\bar{d}$ as obtained from the equal-layered samples. The average spacing shows a slight ($\sim 2\%$) expansion down to $\Lambda = 16.6$ Å and then a sudden contraction. Similar results were also found for the unequal layer thickness samples, the expansion being larger for the thicker Ni sample. We have also reanalyzed earlier data on Cu/Nb superlattices and found a similar expansion for the average lattice parameter but with a smoother order-disorder transition.

While the experimental intensities could have been least-squares fitted with a number of adjustable parameters such as the Ni or Mo interatomic spacings, we preferred to compare the experimental results with those calculated on the basis of two sim-

ple models: In model (i) we assume that there is a uniform expansion of the lattice of Ni and Mo throughout each layer, while in model (ii) we assume that all the expansion is due to a single anomalous spacing at the Mo-Ni interface. For arbitrary Λ, n_1, and n_2 are fractional; hence it was deemed convenient to calculate the intensities numerically rather than analytically. For this purpose we have superimposed sequences of layers containing n' or $n'+1$ atomic planes. These sequences were randomly distributed in the lattice, with a weight factor appropriate to give the experimentally determined Λ.

The scattering amplitude for a large number of atomic planes N was summed up and squared to give $|F|^2$. N was chosen to simulate closely the width of the experimental diffraction lines. The intensities for different sequences of planes and for different values of N were superimposed in order to simulate the real sample. Good agreement with the experimental linewidth was obtained with $N \simeq 50$, which is equivalent to a coherence length of ~ 100 Å. Figure 4 shows the fit of the two models to the experimental intensities of the equilayered superstructures. In the region of Λ where modulation lines appear, the agreement is excellent for both models. Thus, while the basic features common to both models are correct, the analysis of the intensities *per se* is incapable of giving detailed information on the shift of the d spacings from the bulk values of the constituents. The introduction of a larger interlayer disorder in the model calculations (which amounts to a rounding off of the modulation) decreased the intensities of the higher-order satellites too much and caused only a modest (and progressive) broadening of the lines at small Λ; thus it was unable to explain even the sudden increase of linewidth below $\Lambda = 16.6$ Å.

The basic tenets of the model used in analyzing the x-ray intensities have been tested by numerous ancillary observations. These were (a) the determination of the lateral arrangement of nickel and molybdenum in the plane by x-ray diffraction in the transmission geometry, and (b) the determination of the relative thicknesses of the two constituents from small angle x-ray scattering.

In order to determine the lateral arrangements of atoms, we removed two equilayered samples ($\Lambda = 130$ and 50 Å) from the mica substrate and performed systematic θ–2θ scans with the scattering vector at different χ angles (60°–90°) from the normal to the film. Preliminary transmission Laue measurements indicated that the samples were laterally polycrystalline and therefore these measurements were ϕ independent (powderlike).

For $\chi = 70.5°$, we observed a reflection from the (111) nickel plane while at $\chi = 90°$ we observed reflections due to (110) and (200) molybdenum planes. These are precisely the reflections expected if the two constituents preserve their bulk structure. The width of the x-ray diffraction line [$\sim 1.5°$ FWHM (full width at half maximum)] in the plane of the film is attributed to the finite-crystal size effect, independent of the layer thickness. In addition, the thinnest samples show a slight (0.6%) expansion in the Ni spacing and a comparable (0.5%) contraction in the Mo spacing *in the plane.*

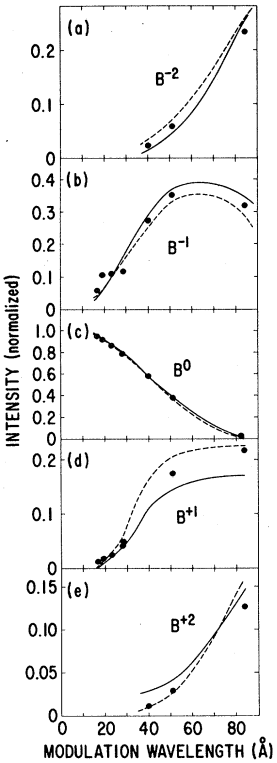

FIG. 4. X-ray intensities normalized as described in the text. The central peak B^0 has satellites at lower 2θ (B^{-2} and B^{-1}) and at higher 2θ (B^{+1} and B^{+2}). Within the experimental errors the data (dots) can be reasonably well fitted by both model (i) solid line and model (ii) dashed line.

As previously mentioned, based on the preparation parameters we estimate the layer thicknesses to be accurate to within $<2\%$ of specification. As an additional check, further x-ray measurements in the reflection geometry were performed at small angles of scattering. In this region, the intensities of the diffraction peaks do not depend on the individual lattice spacings but rather on the variation of the x-ray refractive index between one layer and the next. In particular, for equal layer thickness, the Fourier transform of the composition should only show odd

order peaks. Indeed the even order peaks were undetectable, and the $n=1$ and 3 peaks were clearly observable, indicating square wave modulation.

In conclusion, the crystallographic study of the Ni-Mo samples indicates that these are formed by superstructures of nickel and molybdenum with negligible interdiffusion in the z direction and that these films are polycrystalline in the x-y plane. Also found is a gradual expansion of the average lattice spacing (normal to the laminae) for decreasing Λ, down to a critical value below which it relaxes, with an accompanying loss of crystalline perfection. While the crystallographic analysis *per se* cannot distinguish which part of the crystal is more strained, the fact that the Ni-thick crystals have the larger lattice expansion seems to suggest that nickel is softer, and that the expansion occurs in its lattice.

IV. ELASTIC CONSTANTS

The elastic properties of superlattices have received considerable attention (Refs. 1, 7–10, 13–15, and 21). In particular, there have been several investigations on the dependence of the biaxial modulus, Young's modulus, and flexural modulus as a function of modulation wavelength; some claim a dramatic increase[7–10] while others claim no change at all.[13,14] A decrease of the surface wave velocity has also been reported,[15] but theoretical calculations based on simple elasticity theory[21] indicate that no change should be expected.

We have used Brillouin scattering to measure the velocity of acoustic surface phonons in the Mo/Ni superlattices. The spectra were recorded on a five-pass Fabry-Perot interferometer using ~ 120 mW of 515-nm radiation from a single-mode Ar^+ laser. All spectra were taken with the samples at room temperature. Figure 5 shows the surface wave velocity as a function of modulation wavelength $\Lambda = D_{Mo} + D_{Ni}$ for samples with $D_{Mo} = 3D_{Ni}$ (dots), $D_{Mo} = D_{Ni}$ (crosses), and $D_{Ni} = 3D_{Mo}$ (triangles). The error bars are given by the reproducibility of the results and the number of data points taken on each sample. We should point out that most of the observed Brillouin peaks were broader than the instrumental resolution and in certain cases (some samples in the range 60 Å $\leq \Lambda \leq$ 300 Å) consisted of a doublet. The polarization features of each component of the doublet are those expected for surface phonons, and the peak positions are independent of magnetic field up to 5 kG. Magnons have been observed at higher frequencies than the phonons and are the subject of further investigations. We conclude that the "phonon doublet" is not due to phonon-magnon coupling, and that the broad peak observed in most cases is due to an unresolved doublet. The position

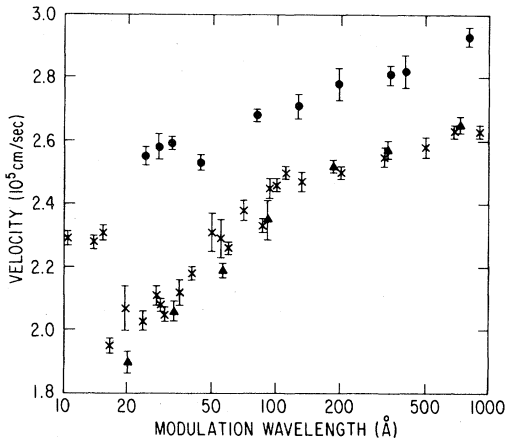

FIG. 5. Surface wave velocity as a function of modulation wavelength ($\Lambda = D_{Mo} + D_{Ni}$) for samples with $D_{Mo} = 3D_{Ni}$ (dots), $D_{Mo} = D_{Ni}$ (crosses), and $D_{Ni} = 3D_{Mo}$ (triangles).

of the Brillouin peak in this paper is defined as the peak position when only one peak is present and as the midpoint of the doublet when two are observed. We should also point out that the doublet splitting, when observed, is about half that of the changes as a function of Λ.

Returning now to Fig. 5, we note that the dip in the sound velocity for $D_{Ni} = D_{Mo}$ (crosses) occurs for $\Lambda \simeq 18$ Å. For $D_{Mo} = 3D_{Ni}$ (dots), there is evidence of a dip between $\Lambda = 35$ and 45 Å. For $D_{Ni} = 3D_{Mo}$ (triangles), the velocity decreases down to $\Lambda = 20$ Å and is consistent with a dip at $\Lambda \leq 20$ Å. Together, all samples show a behavior in the velocity consistent with the interpretation that the material undergoes a structural transition for a critical thickness of nickel ($D_{Ni} \simeq 8$ Å) rather than at a certain value of the modulation wavelength.

A more quantitative proof of the statement above can be given by considering a model intermediate to those presented in the discussion of the x-ray data. Suppose that at every interface there is a layer of thickness D_L (a) which is independent of D_{Ni} or D_{Mo} and (b) if isolated would support a Rayleigh wave of velocity v_L. The velocity v of the surface wave in the layered structure can then be approximated by[15]

$$\frac{\Lambda}{v^2} = \frac{D_1}{v_1^2} + \frac{D_2}{v_2^2} + \frac{D_L}{v_L^2} , \tag{3}$$

where v_1 and v_2 are the Rayleigh wave velocities and D_1 and D_2 are the effective thicknesses of Ni and Mo, respectively. We consider three cases: (a) the interface layer consists only of a modification of Mo, i.e., $D_1 = D_{Ni}$ and $D_2 = D_{Mo} - D_L$, (b) the interface layer is composed of equal thicknesses of Mo

and Ni, i.e., $D_1 = D_{Ni} - \frac{1}{2}D_L$ and $D_2 = D_{Mo} - \frac{1}{2}D_L$, and (c) the interface layer consists only of a modification of the Ni, i.e., $D_1 = D_{Ni} - D_L$ and $D_2 = D_{Mo}$.

We then choose D_L and v_L in order to obtain a minimum at $\Lambda = 22$ Å with velocity $v = 2.0 \times 10^5$ cm/sec in accordance with the experiments for the case of equal layer thickness. The velocities for Ni and Mo are taken to be $v_1 = 2.42 \times 10^5$ cm/sec as measured in a thick Ni film and $v_2 = 3.27 \times 10^5$ cm/sec obtained from the average surface wave velocity calculated for a Mo(110) surface. For the above cases we obtain (a) $D_L = 11$ Å, $v_L = 1.74 \times 10^5$ cm/sec, (b) $D_L = 22$ Å, $v_L = 2.0 \times 10^5$ cm/sec, and (c) $D_L = 11$ Å, $v_L = 1.57 \times 10^5$ cm/sec.

For $D_{Mo} = D_{Ni}$, these three models all yield essentially the same Λ dependence of the velocity and are shown by the solid lines in Fig. 6. However, for the unequal thickness layers the three models yield different results as shown by the dashed and dotted lines for $D_{Mo} = 3D_{Ni}$ and $D_{Ni} = 3D_{Mo}$, respectively. A comparison with the experimental data indicates the best agreement with model (c) i.e., $D_1 = D_{Ni} - D_L$ and $D_2 = D_{Mo}$. Of course, the upturn observed in the experimental data cannot be reproduced by the present calculation. However, this behavior is consistent with the interpretation that the upturn is a consequence of a sudden crystal transformation when $D_{Ni} \sim 8$ Å, as was concluded from x-ray measurements discussed in Sec. III.

We conclude therefore that it is highly probable that the observed velocity softening is due to changes in the Ni layers. We also point out that the velocity softening previously observed in Nb/Cu superlattices[15] has likewise been found to correlate with an expansion of the average lattice parameter.

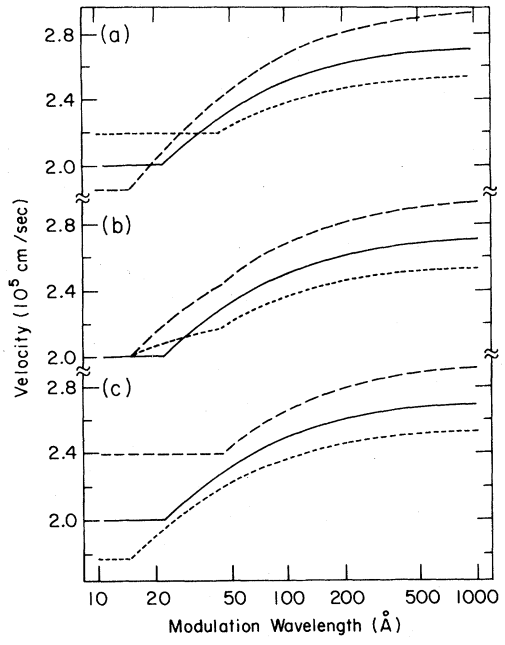

FIG. 6. Surface wave velocity as calculated from models in which parts of the Mo and Ni layers which are closest to interfaces are modified. Case (a): Only part of each Mo layer is changed. Case (b): An equal amount of each Mo and Ni layer is changed. Case (c): Only part of each Ni layer is changed. The curves are for samples with $D_{Mo} = D_{Ni}$ (solid line), $D_{Mo} = 3D_{Ni}$ (dashed line), and $D_{Ni} = 3D_{Mo}$ (dotted line).

V. ELECTRICAL RESISTIVITY

The resistivity of the Mo/Ni material was determined from four-point resistance measurements of samples with well-defined geometric shapes. A four-point bridge structure was formed by standard photolithographic techniques. Chemical etching was done in a solution of nitric acid and distilled water. The resulting conduction channel had the approximate dimensions 1 μm $\times$ 0.3 mm $\times$ 4.3 mm. The resistances of the etched samples on sapphire substrates were measured using a standard ac lock-in method with 10 μA passing through the samples at 25 Hz. A closed-cycle refrigerator with a temperature-controlled cooling stage permitted measurements at temperatures from 8 to 300 K.

The electrical resistivity for equal layer thickness samples is shown in Fig. 7. At any given temperature there is an increase in resistivity as the modulation wavelength Λ decreases. Figure 8 shows the temperature coefficient of resistivity (TCR) averaged over the temperature range 100–300 K for equal and unequal layer thickness samples. The average TCR is positive at large Λ and becomes smaller with decreasing Λ. For the equal layer

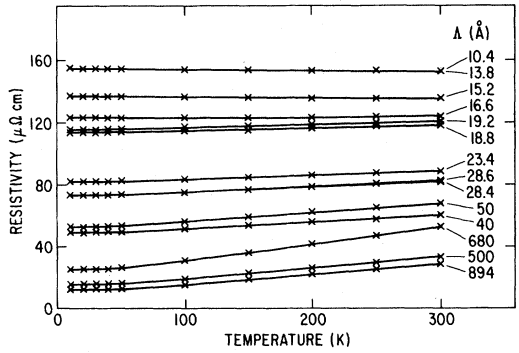

FIG. 7. Electrical resistivity of Mo/Ni superlattice samples. The uncertainty in the dimensions of the samples is less than 10%, resulting in a systematic uncertainty in the absolute value of ρ of less than 10%.

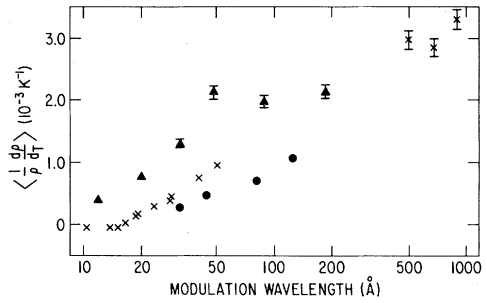

FIG. 8. Temperature coefficient of resistivity averaged over the temperature range 100–300 K for Mo/Ni superlattice samples with $D_{Mo}=3D_{Ni}$ (dots), $D_{Mo}=D_{Ni}$ (crosses), and $D_{Ni}=3D_{Mo}$ (triangles).

thickness samples the average TCR becomes zero at $\Lambda\approx 16$ Å and with further decreases in Λ becomes a constant negative value. This anomaly of the average TCR—the transition from metalliclike behavior to non-metallic-like behavior—has a striking correspondence with the structural and elastic anomalies noticed in the same samples. In particular, the x-ray analysis in Sec. III and surface-phonon study in Sec. IV seem to indicate that the structural changes are due to a systematic Ni lattice expansion as Λ is decreased followed by a contraction at $\Lambda\approx 16$ Å. In addition, the Mo layers seem to play a passive role for all values of Λ. This can also be concluded from the average TCR values. In Fig. 8 the average TCR values for the $D_{Ni}=3D_{Mo}$ and $D_{Mo}=3D_{Ni}$ samples extrapolate to zero for $\Lambda\approx 9$ and 20 Å, respectively. The average TCR for equal layer thickness samples crosses through zero at $\Lambda\approx 16.6$ Å. We can well conclude that the average TCR behavior is dominated by the Ni layers and that the average TCR becomes zero at $D_{Ni}\approx 8$ Å.

VI. CONCLUSIONS

From the present work on Mo/Ni superlattices the following conclusions can be made.

(1) bcc/fcc superlattice structures can be stabilized with materials which have a noneutectic equilibrium binary/phase diagram, in particular Mo and Ni. This is in contrast with the previously studied Nb/Cu superlattices where Nb and Cu are eutectic.

(2) The data show an interesting correlation between three different properties of Mo/Ni superlattices: structure, elastic constant, and electrical resistivity. (a) For $D_{Ni}=D_{Mo}\approx 8$ Å x-ray studies show that the material undergoes what appears to be a rather sudden *structural change* from an ordered to a disordered structure with a precursor effect in which the average lattice spacing gradually increases by about 2%. $D_{Ni}=3D_{Mo}$ samples have a larger average lattice expansion than $D_{Mo}=3D_{Ni}$, suggesting that this structural change is induced by the response of the nickel layer to strain. (b) There is a minimum in the surface wave velocity at $D_{Ni}=D_{Mo}\approx 9$ Å. Measurements on samples with $D_{Ni}=3D_{Mo}$ and $D_{Mo}=3D_{Ni}$ indicate that the velocity softening is probably due to changes in the Ni layers. (c) Electrical resistivity measurements show a change from positive TCR to negative TCR for samples with $D_{Ni}=D_{Mo}$. The TCR of samples with $D_{Ni}=3D_{Mo}$ and $D_{Mo}=3D_{Ni}$ show that the change in sign of TCR occurs at $D_{Ni}\approx 8$ Å and does not depend on D_{Mo}.

(3) The relationship between the expansion of the lattice, the structural transformation, the elastic constant, and the temperature coefficient of resistivity has now been observed in both Nb/Cu and Mo/Ni superlattices.[5,15,17] Observations on Nb/Cu were made only on samples with layers of equal thickness. Here measurements on Mo/Ni with $D_{Mo}=3D_{Ni}$ and $D_{Ni}=3D_{Mo}$ indicate that the changes in the structure, surface-phonon velocity, and TCR are due to a critical thickness in one of the constituents (Ni in our case) and not due to the number of interfaces.

As a possible explanation for the correlation between lattice expansion and phonon softening, we note that if the lattice is forced to expand it is expected that at a certain critical value of stress the crystal will either break or suffer a phase change. This has previously been obesrved in static as well as molecular dynamics calculations[22,23] for a Ni single crystal strained along a [001] axis. These calculations however, do not show a softening of Young's modulus along the [001] axis up to the breaking point. This difference may be due to the fact that in our case the lattice is strained along the close-packed [111] direction and not along the [001] axis. Further molecular dynamics calculations are underway to check these points in detail.

In summary, we have found anomalies in the structural, elastic, and transport properties of Mo/Ni superlattices. We interpret our results to indicate that the Ni layers are responsible for the anomalies and present arguments, which would explain the correlation between the structural and elastic properties. No simple explanation has been found relating the changes in electrical properties to the changes in structure and elastic properties or to the expansion of the nickel lattice.

ACKNOWLEDGMENTS

We wish to thank A. Rahman and J. Zak for helpful discussions. This work was supported by the U.S. Department of Energy and the U.S. Office of Naval Research under Grant No. N00014-80-F-0074.

*Present address: Department of Physics and Astronomy, Northwestern University, Evanston, Illinois 60201.

†Present address: Departments of Physics and Optical Sciences and Arizona Research Laboratories, University of Arizona, Tucson, Arizona 85721.

[1]For a recent review see A. C. Gossard, Thin Solid Films 57, 3 (1979).

[2]J. E. Hilliard, in *Modulated Structures—1979 (Kailua Kona, Hawaii),* Proceedings of the International Conference on Modulated Structures, edited by J. M. Cowley, J. B. Cohen, M. B. Salamon, and B. J. Wuensch (AIP, New York, 1979), p. 407.

[3]S. M. Durbin, J. E. Cunningham, M. E. Mochel, and C. P. Flynn, J. Phys. F 11, L223 (1981).

[4]I. K. Schuller and C. M. Falco, in *Inhomogeneous Superconductors—1979 (Berkeley Springs),* Proceedings of the Conference on Inhomogeneous Superconductors, edited by D. U. Gubser, T. L. Francavilla, J. R. Leibowitz, and S. A. Wolf (AIP, New York, 1980), p. 197.

[5]I. K. Schuller, Phys. Rev. Lett. 44, 1597 (1980).

[6]S. T. Ruggiero, T. W. Barbee, Jr., and M. R. Beasley, Phys. Rev. Lett. 45, 1299 (1980).

[7]T. Tsakalakos, Ph.D. thesis, Northwestern University, 1977 (unpublished).

[8]W. M. C. Yang, T. Tsakalakos, and J. E. Hilliard, J. Appl. Phys. 48, 876 (1977).

[9]G. Henein, Ph.D. thesis, Northwestern University, 1979 (unpublished).

[10]L. R. Testardi, R. H. Willens, J. T. Krause, D. B. McWhan, and S. Nakahara, J. Appl. Phys. 52, 510 (1981).

[11]E. M. Gyorgy, J. F. Dillon, Jr., D. B. McWhan, L. W. Rupp, Jr., L. R. Testardi, and P. J. Flanders, Phys. Rev. Lett. 45, 57 (1980).

[12]J. Q. Zheng, C. M. Falco, J. B. Ketterson, and Ivan K. Schuller, Appl. Phys. Lett. 38, 424 (1981).

[13]B. S. Berry and W. C. Pritchet, Thin Solid Films 33, 19 (1976).

[14]H. Itozaki, Ph.D. thesis, Northwestern University, 1982 (unpublished).

[15]A. Kueny, M. Grimsditch, K. Miyano, I. Banerjee, Charles M. Falco, and Ivan K. Schuller, Phys. Rev. Lett. 48, 166 (1982).

[16]Indrajit Banerjee, Ph.D. thesis, Northwestern University, 1982 (unpublished).

[17]T. R. Werner, Indrajit Banerjee, Q. S. Yang, Charles M. Falco, and Ivan K. Schuller, Phys. Rev. B 26, 2224 (1982).

[18]R. P. Elliot, *Constitution of Binary Alloys, First Supplement* (McGraw-Hill, New York, 1965), p. 253; F. A. Shunk, *Constitution of Binary Alloys, Second Supplement* (McGraw-Hill, New York, 1969), p. 515.

[19]A. Guiner, *X-Ray Diffraction in Crystals, Imperfect Crystals and Amorphous Bodies,* translated by P. Lorrain and D. Saint Marie Lorrain (Freeman, San Francisco, 1963), p. 124.

[20]D. T. Cramer and J. T. Weber, Los Alamos National Laboratory Report No. LA-3056 (unpublished).

[21]A. Kueny and M. Grimsditch, Phys. Rev. B 26, 4699 (1982).

[22]M. Parrinello and A. Rahman, J. Appl. Phys. 52, 7182 (1981).

[23]F. Milstein and B. Farber, Phys. Rev. Lett. 44, 277 (1980).